Elastic/anelastic behaviour during the phase transition in spinel $LiMn_2O_4$

1995 J. Phys.: Condens. Matter 7 9755

(http://iopscience.iop.org/0953-8984/7/50/010)

J. Phys.: Condens. Matter 7 (1995) 9755–9764. Printed in the UK

Elastic/anelastic behaviour during the phase transition in spinel $LiMn_2O_4$

Jun Sugiyama†, Toshiyuki Tamura and H Yamauchi‡

Superconductivity Research Laboratory, International Superconductivity Technology Centre, 10-13 Shinonome 1-chome, Koto-ku, Tokyo 135, Japan

Received 10 July 1995, in final form 26 September 1995

Abstract. Both the Young's modulus sound velocity (V_E) and the internal friction (Q^{-1}) have been measured for a polycrystalline sample of $LiMn_2O_4$ in the temperature range between 35 and 350 K, using a vibrating-reed technique. The resonance frequency (f_r) employed for the measurement ranged from 0.81 kHz to 2.69 kHz at 300 K. At $f_r(300\ K) = 0.81$ kHz, as temperature is lowered from 350 K, V_E decreases down to 225 K (T_A). Then, V_E increases rapidly but monotonically with lowering temperature, though the magnitude of the slope ($-dV_E/dT$) reduces. The overall increase in the velocity between T_A and 100 K is about 68%. In the Q^{-1}-versus-T curve, a large peak is clearly observed at around 210 K, as is the forming of a large shoulder on the low-temperature side; additionally, there exists a small Q^{-1} peak at around 120 K, though V_E indicates no significant change at around 120 K. Furthermore, both the V_E-versus-T curve and the Q^{-1}-versus-T curve shift toward the higher-temperature side, by ~45 K and ~25 K, as $f_r(300\ K)$ is increased from 1.32 kHz to 2.69 kHz. The observed elastic anomalies suggest that a phase transition occurs at temperatures below 290 K. This phase transition is probably due to an ordering of Mn^{3+} and Mn^{4+} ions on the octahedral 16d site in the spinel lattice. On the other hand, the origin of the Q^{-1} peak is considered to lie in a stress-induced relaxation of the distributions of Mn ions or Li ions.

1. Introduction

The spinel-type compound, $LiMn_2O_4$, is known to be one of the most promising candidates for cathode materials of rechargeable lithium batteries [1–4]. At ambient temperature, the crystal structure of $LiMn_2O_4$ belongs to the $Fd3m$ space group [5] of a cubic system; lithium ions occupy the tetrahedral 8a site, manganese ions the octahedral 16d site and oxygen ions the 32e site [6]. Since the average valence of manganese ions in $LiMn_2O_4$ is 3.5, the same amounts of Mn^{3+} and Mn^{4+} ions are distributed randomly on the 16d site. That is, the distribution of cations in $LiMn_2O_4$ can be represented by the following ionic formula: $(Li^+)_{8a}[Mn^{3+}Mn^{4+}]_{16d}O_4^{2-}$ [6]. According to neutron and x-ray diffraction analyses [1, 7–11], the Mn_2O_4 spinel framework remains during the insertion of excess lithium into $LiMn_2O_4$ as well as during lithium extraction from the stoichiometric material. In other words, the process of the insertion and the extraction of Li^+ is found to be via intercalation of Li^+ between two layers consisting of MnO_6 octahedra. Therefore, the diffusion coefficient

† Present address: Toyota Central Research and Developments Laboratories Inc., 41-1 Yokomichi, Nagakute, Aichi 480-11, Japan.

‡ Present address: Centre for Ceramic Research, Tokyo Institute of Technology, Nagatsuta, Midori-ku, Yokohama 226, Japan.

0953-8984/95/509755+10$19.50

of the intercalated Li^+ is considered to strongly depend on the structure of the area between two adjacent MnO_6 layers.

Since the elastic properties sensitively depend on the lattice distortion, the elastic constants are considered to be good indicators for the evaluation of performance of cathode materials. Furthermore, there is a possibility that the activation energy for intercalating Li^+ ions can be estimated from the measurement of anelastic relaxation, as proposed for the case of quartz which contains alkali ions [12]. Nevertheless, to the authors' knowledge, there are no elastic/anelastic studies on $LiMn_2O_4$, though there have been numerous studies on structural and electrochemical properties of $LiMn_2O_4$ [1–4, 7–11]. Unfortunately, single-crystal samples of $LiMn_2O_4$ are currently not available, because $LiMn_2O_4$ decomposes at around 950 °C [6] below its melting point. Thus, in order to understand the lattice distortion due to Li intercalation, we studied the elastic/anelastic properties of polycrystalline $LiMn_2O_4$ samples using a vibrating-reed technique [13–17]. Here, we report the Young's modulus sound velocity (V_E) and the internal friction (Q^{-1}) of $LiMn_2O_4$ with respect to both temperature and frequency.

2. *Experimental procedure*

Polycrystalline samples of $LiMn_2O_4$ were synthesized by a solid-state reaction technique using reagent-grade Li_2CO_3 and MnO_2 powders. The powders were thoroughly mixed by a planetary ball mill using ethanol as the solvent. After drying, the mixture was calcined three times at 800 °C for 8 h in a 20% O_2–N_2 gas mixture flow. After grinding, the calcined powder was pressed into rectangular bars using a cold isostatic press (CIP) apparatus. And then, the bars were sintered at 900 °C for 8 h in a 20% O_2–N_2 gas mixture flow. The sample was furnace cooled to room temperature with a rate of ~4 °C min^{-1}.

Powder x-ray diffraction analysis indicated that the sample was a single phase of a cubic spinel structure with the lattice parameter $a \sim 0.824$ nm. According to a chemical analysis using inductively coupled plasma (ICP) spectrometry, the cation ratio in the sample was: Li/Mn = 0.95/2.00. The electrical resistivity (ρ) of the sample was measured by a dc four-probe method. The magnetic susceptibility (χ) was measured using a superconducting quantum interference device (SQUID) magnetometer in a magnetic field of $H = 1$ T.

For vibrating-reed measurements [13–17], samples were polished into thin plates of dimensions $\sim 15 \times 2 \times 0.2$ mm^3. In order to make the sample conductive, gold was sputtered on the surface to a thickness of ~500 nm.

The mechanical resonance frequency (f_r) for the fundamental mode of a thin bar whose one end is clamped rigidly and other end is free is given by [13–17]

$$f_r = 0.1615 \frac{t}{\ell^2} V_E \tag{1}$$

$$V_E = \sqrt{E/d} \tag{2}$$

where ℓ is the length of the reed, t the thickness, V_E Young's modulus sound velocity, E Young's modulus and d the density. The internal friction (Q^{-1}) of the reed is expressed as

$$Q^{-1} = \Delta f / f_r \tag{3}$$

when $\Delta f / f_r \ll 1$, in which Δf is the full width at $\sqrt{1/2}$ maximum of the resonance peak.

3. Results

Figures 1(a)–1(c) show the temperature dependences of the change of V_E ($\Delta V_E/V_E$(300 K)), Q^{-1} and the magnitude of slope of V_E ($-dV_E/dT$). The value of f_r employed for the measurement was 0.81 kHz at 300 K. There were no marked differences between the data obtained on cooling and on heating. As temperature was lowered from 350 K, V_E decreased monotonically down to 225 K (T_A); in other words, V_E softened by about 5% from 350 K to T_A. Then, V_E changed sign of the slope, dV_E/dT, from positive to negative at T_A, increased rapidly with lowering temperature and levelled off at temperatures below 50 K. The overall stiffening of the velocity was about 63% between T_A and 50 K.

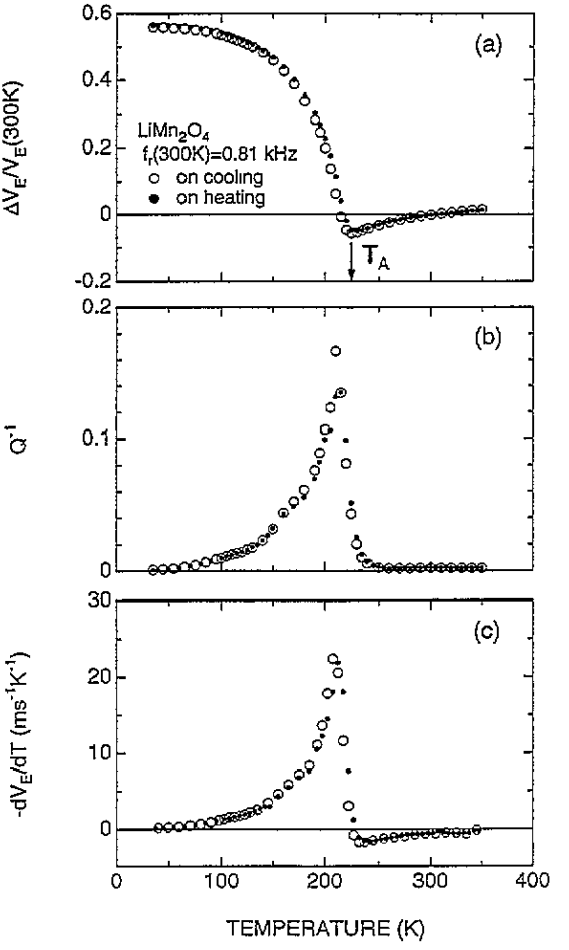

Figure 1. Temperature dependences of (a) the change of the Young's modulus sound velocity ($\Delta V_E/V_E$(300 K)), (b) the internal friction (Q^{-1}), and (c) the magnitude of the slope of V_E ($-dV_E/dT$) for $LiMn_2O_4$; open circles represent data obtained on cooling and solid circles on heating. The resonance frequency (f_r) employed for the measurement was 0.81 kHz at 300 K.

On the other hand, as temperature was lowered from 350 K, Q^{-1} rapidly increased at around 250 K, having an intense peak at 210 K (T_{peak}), and forming a large shoulder on the low-temperature side (see figure 1(b)). In addition, there appeared a small peak at around 160 K, though V_E showed no obvious change at around 160 K. At temperatures below

120 K, Q^{-1} decreased monotonically with lowering temperature.

In an attempt to understand the temperature dependence of V_E, the magnitude of the slope, $-dV_E/dT$, is plotted in figure 1(c) as a function of temperature. It is seen that the $(-dV_E/dT)$-versus-T curve is akin to the Q^{-1}-versus-T curve (see figure 1(b)). Such similarity between the two curves had been reported for polycrystalline samples of superconducting $Pb_{(1+x)/2}Cu_{(1-x)/2}(Sr_{1-y}Ca_y)_2(Y_{1-x}Ca_x)Cu_2O_{7+\delta}$ [17].

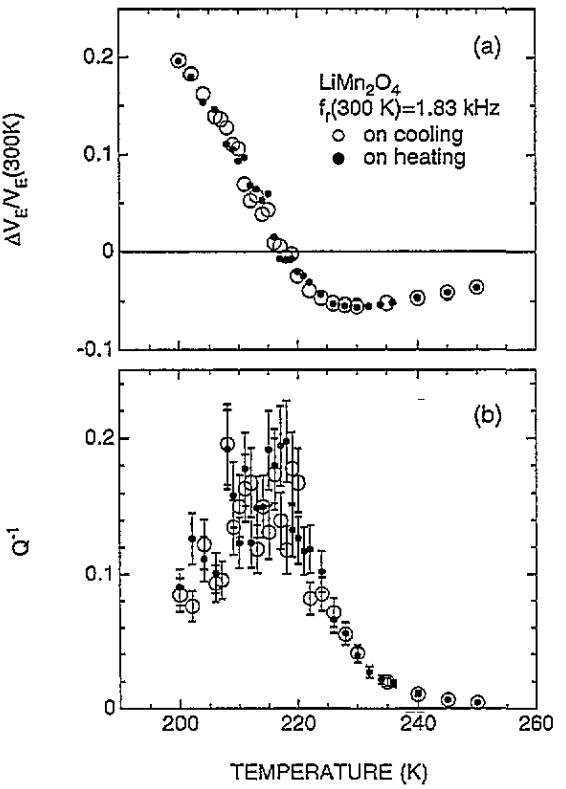

Figure 2. Magnification of the temperature dependences of (a) $\Delta V_E/V_E$(300 K), and (b) Q^{-1} at temperatures in the vicinity of T_A (=230 K); f_r(300 K) = 1.83 kHz; open circles represent data obtained on cooling and solid circles on heating.

Figures 2(a) and 2(b) show the temperature dependences of $\Delta V_E/V_E$(300 K) and Q^{-1} at temperatures in the vicinity of T_A. The value of f_r at 300 K was 1.83 kHz. The accuracy of the measured Q^{-1} was lower at temperatures below 220 K than that above 220 K. This was because the intensity of the resonance peak became extremely weak due to a large elastic loss at temperatures below T_A. As seen in figure 2, the values of T_A and T_{peak} were found to be 230 K and 215 K, respectively; thus, making comparison with the result obtained at $f_r(300\ K) = 0.81$ kHz, both values of T_A and T_{peak} increased by 5 K.

Figures 3(a) and 3(b) show $\Delta V_E/V_E$(300 K)-versus-T curves and Q^{-1}-versus-T curves obtained at four different frequencies, i.e., $f_r(300\ K) = 1.32$ kHz, 1.68 kHz, 2.48 kHz and 2.69 kHz, respectively, in the temperature range between 150 K and 350 K. As f_r(300 K) was increased from 1.32 kHz to 2.69 kHz, not only the Q^{-1}-versus-T curve but also the $\Delta V_E/V_E$(300 K)-versus-T curve shifted toward the higher-temperature side, by ~25 K and ~45 K. It should be noted that $T_{peak} < T_A$ for each of the data obtained at different values of f_r. Moreover, the height of the Q^{-1} peak decreased with increasing f_r(300 K). In order to understand the frequency dependences of Q^{-1}, we have plotted in figure 4 the normalized Q^{-1} (Q^{-1}/Q^{-1}_{max})-versus-T^{-1} curves at temperatures in the vicinity of T_{peak}. It is clearly seen that, as f_r(300 K) was increased from 1.32 kHz to 2.69 kHz, the Q^{-1} peak shifted

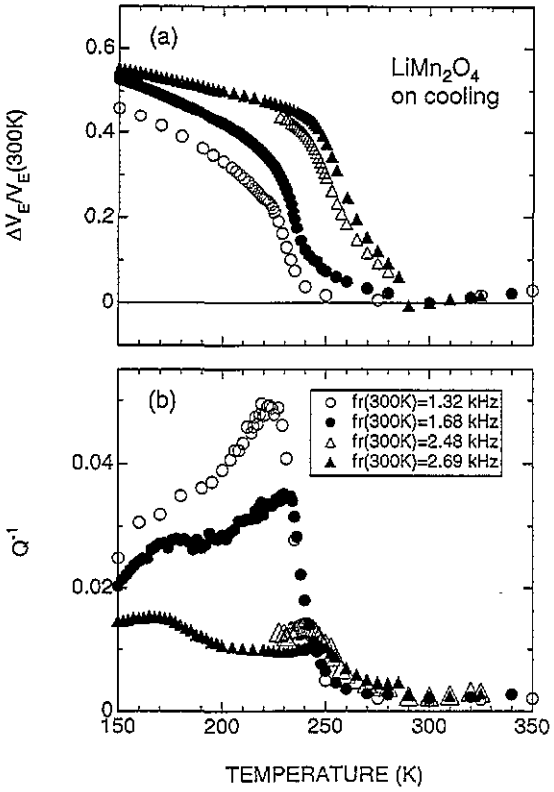

Figure 3. Magnification of the temperature dependences of (a) $\Delta V_E/V_E$(300 K), and (b) Q^{-1} at four different frequencies; f_r(300 K) = 1.32, 1.68, 2.48 and 2.69 kHz, respectively.

toward the higher-temperature side by 22 K. In addition, the peak width seems to become large with increasing f_r(300 K); the reason for this will be discussed later.

In order to estimate the absolute value of V_E [15], we have plotted in figure 5 the relationship between ℓ and $\sqrt{t/f_r}$ at 300 K measured for several sample pieces with different dimensions. Based on a linear fit, the slope of ℓ yields $\sqrt{0.1615V_E}$ in accordance with equation (1); thus, V_E was estimated to be 1960 m s^{-1}. Using this value and $d = 2.66$ g cm^{-3} in equation (2), we obtain $E(300\ \text{K}) = 1.02 \times 10^{10}$ N m^{-2}. Then, assuming that Poisson's ratio (ν) for $LiMn_2O_4$ takes a typical value ($\nu = 0.3$), we employed the following relationship [18] for the corrections due to pores:

$$E = E_0\left(1 - 1.9P + 0.9P^2\right) \tag{4}$$

where E_0 is Young's modulus of a pore-free sample and P the porosity. Since the theoretical density (d_0) for $LiMn_2O_4$ is 4.28 g cm^{-3} [5], P would be roughly given by $P = 1 - (d/d_0) = 38\%$. Therefore, E_0 was estimated to be 0.25×10^{11} N m^{-2} at 300 K. This value was considerably smaller than the value for $Fe_{1.6}Mn_{1.18}O_4$ of a spinel structure, i.e., $E_{[110]} = 1.45 \times 10^{11}$ N m^{-2} [19]. This is probably due to the effect of microcracks in the sample, as proposed for polycrystalline samples of $YBa_2Cu_3O_7$ by Ledbetter [20, 21].

4. Discussion

First, we should note that all the measurements were carried out using polycrystalline samples of $LiMn_2O_4$. Therefore, the present data include the effects due to pores, grain boundaries and/or structural domains in the sample. However, it is unlikely that the

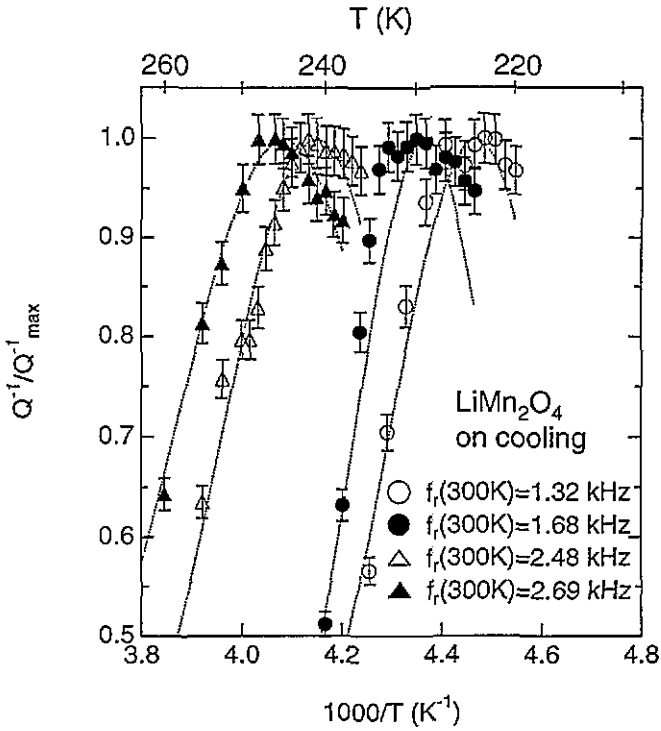

Figure 4. The dependence of normalized Q^{-1} (Q^{-1}/Q^{-1}_{max}) on the reciprocal temperature (T^{-1}) for $LiMn_2O_4$ at four different frequencies; f_r(300 K) = 1.32, 1.68, 2.48 and 2.69 kHz.

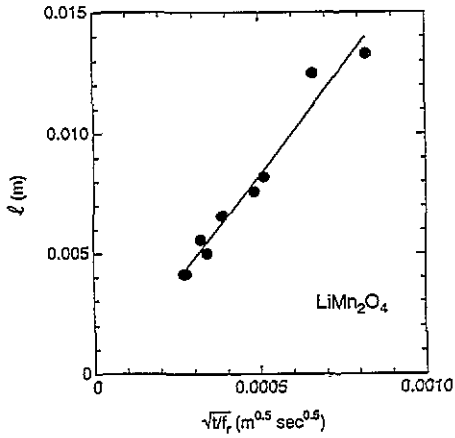

Figure 5. The relationship between ℓ and $\sqrt{t/f_r}$ at 300 K measured for several sample pieces of $LiMn_2O_4$; where ℓ is the length of the reed and t the thickness.

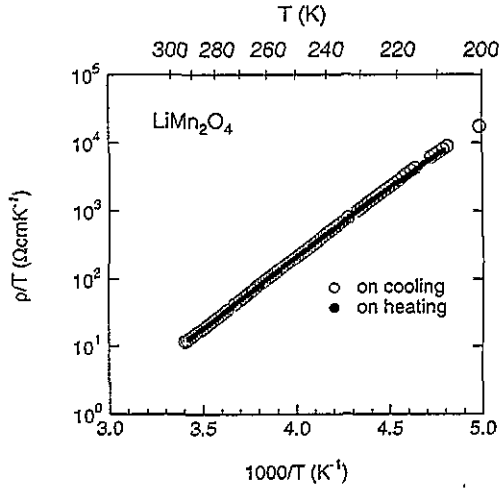

Figure 6. The relationship between $\log(\rho/T)$ and T^{-1} for $LiMn_2O_4$; where ρ is the resistivity.

large change in $\Delta V_E/V_E$(300 K) at temperatures below 290 K and the sharp Q^{-1} peak at temperatures below 245 K are caused by such effects. Furthermore, there were no marked

differences between the data obtained on cooling and on heating, even at temperatures around T_A. Hence, the present results suggest that $LiMn_2O_4$ undergoes a phase transition at temperatures below 290 K. Unfortunately, no reports are available at present for the study on temperature dependence of the crystal structure of $LiMn_2O_4$. Here, we discuss the origin of this phase transition and/or the Q^{-1} peak using the following two most probable models: (A) ordering of Mn^{3+} and Mn^{4+} ions on the octahedral 16d site and (B) movement of Li^+ ions on the tetrahedral 8a site.

4.1. Model A: ordering of Mn^{3+} and Mn^{4+} ions on the octahedral 16d site

It is known that one spinel compound, Fe_3O_4 (magnetite), undergoes a continuous phase transition at around 125 K (T_V) [22]; this transition is usually called the Verwey transition, which is attributed to an ordering of Fe^{2+} and Fe^{3+} ions on the octahedral 16d site in $(Fe^{3+})_{8a}[Fe^{2+}Fe^{3+}]_{16d}O_4$. As temperature is lowered from 300 K, $E_{[111]}$ decreases monotonically and suddenly increases at T_V. Moreover, there are two sharp peaks at around 110 K and 40 K in the $Q^{-1}_{[111]}$-versus-T curve. The two $Q^{-1}_{[111]}$ peaks are due to stress-induced relaxation of the distribution of Fe^{2+} and Fe^{3+} [23]. The relaxation time ($\tau = 1/(2\pi f_r)$) is known to obey the well-known Arrhenius relation

$$\tau = \tau_0 \exp(W/k_B T) \tag{5}$$

in which τ_0 is a constant, W the activation energy for the process, k_B Boltzmann's constant and T the absolute temperature. For the $Q^{-1}_{[111]}$ peak at around 110 K, W and τ_0^{-1} were estimated to be 0.36 eV per unit process and 4.3×10^{11} Hz [24]; for the peak at around 40 K, $W = 0.055$ eV per unit process and $\tau_0^{-1} = 6.5 \times 10^{23}$ Hz [24]. Furthermore, similar dependences of $E_{[110]}$ and $Q^{-1}_{[110]}$ on temperature had been reported for a spinel-type compound $Fe_{1.6}Mn_{1.18}O_4$ [19] (Mn ferrite); two Q^{-1} peaks were observed at around 260 K and 40 K, while $E_{[110]}$ exhibited a minimum at around 290 K and then increased with decreasing temperature. For the peak at around 260 K, it was reported that $W = 0.27 - 0.34$ eV per unit process and $\tau_0^{-1} = 10^{12}$ Hz, though both values strongly depended on the composition and/or the homogeneity of the sample. Additionally, for the peak at around 40 K, it was reported that $W = 0.03$ eV per unit process and $\tau_0^{-1} = 10^{10}$ Hz.

It is worth noting that the temperature dependences of $E_{[111]}$ and $Q^{-1}_{[111]}$ of magnetite and of $E_{[110]}$ and $Q^{-1}_{[110]}$ of Mn ferrite are parallel to the present data for $LiMn_2O_4$. Therefore, the phase transition at T_A in $LiMn_2O_4$ can be attributed to an ordering of Mn^{3+} and Mn^{4+} on the octahedral 16d site. The Q^{-1} peak observed just below T_A is most likely to be caused by a stress-induced relaxation of the distributions of Mn^{3+} and Mn^{4+} among the 16d sites; that is, the larger Mn^{3+} would tend to orient in the direction of tensile stresses, while the smaller Mn^{4+} would tend to orient in the direction of compressive stresses. However, as seen in figure 4, the width of the Q^{-1} peak was found to increase with increasing f_r. This implies that the relaxation time does not obey equation (5); also, it looks difficult to apply the Debye equation [13] to explain the temperature dependence of Q^{-1}. Indeed, if we employed equation (5) for the present data, the values of W and τ_0^{-1} would be estimated to be 0.14 eV per unit process and 1.5×10^7 Hz, based on a linear fit to the relation between $\log(f_{r,peak})$ and $1/T_{peak}$. This value of W is rather small compared with those for magnetite and Mn ferrite; moreover, the value of τ_0^{-1} is about five orders of magnitude smaller than those for magnetite and Mn ferrite, and seems to be too small to explain. Hence, the stress-induced relaxation of $LiMn_2O_4$ is considered to have a varying activation energy with respect to frequency and/or temperature. In other words, the relaxation process

seems to strongly correlate with the change in the crystal structure.

If an ordering of Mn^{3+} and Mn^{4+} occurs below T_A, both electronic and magnetic structures would be altered at T_A. As a result, both resistivity (ρ) and magnetic susceptibility (χ) should exhibit clear anomalies at around T_A; indeed, such anomalies at around T_V were observed for magnetite [25]. For $LiMn_2O_4$, both ρ and χ exhibited no clear anomalies at around T_A, as shown in figures 6 and 7. However, a small anomaly was detected at 288 K by the χ measurement (see figure 7(b)). The electron configuration of Mn^{3+} in $LiMn_2O_4$ is represented as $t_{2g}^3e_g^1$, i.e., a high-spin configuration, while that of Mn^{4+} is represented as $t_{2g}^3e_g^0$. Generally, Mn^{3+} ions in a high-spin state give a tetragonal distortion due to a Jahn–Teller effect. Furthermore, interactions between Mn ions are too weak to give an itinerant-electron bandwidth [26]. Consequently, $LiMn_2O_4$ is known to be a small-polaron semiconductor [26, 27], because the e_g electrons are localized and coupled with the tetragonal distortion of Mn^{3+} at ambient temperature. Even in an ordered state at temperatures below T_A, the e_g electrons are considered also to be localized; thus, the change in χ at T_A might be rather small. Indeed, $TbVO_4$ and $DyVO_4$ undergo structural phase transitions at 34 K and 15 K, respectively, due to a cooperative Jahn–Teller effect [28, 29]; for each of these compounds, as the temperature is lowered, a small decrease in χ is observed at a critical temperature (T_c), though the elastic constant exhibits a large softening at T_c. Finally, the activation energy for dc $\rho(W_\rho)$ was estimated to be 0.41 eV at temperatures above 220 K using the relationship, $\rho/T \propto \exp(W_\rho/k_BT)$. The value of W_ρ is about three times larger than that of W (=0.14 eV). This discrepancy also suggests that the mechanism of the Q^{-1} peak cannot be explained using a simple stress-induced relaxation phenomenon described by equation (5).

As f_t increased, the $\Delta V_E/V_E$(300 K)-versus-T curve also shifted toward the higher-temperature side, as seen in figure 3(a). This indicates the possibility that the phase transition at T_A is discontinuous, though there were no marked differences between the data obtained on cooling and on heating. Moreover, it seems difficult to determine the value of T_A, on the basis of just the present elastic/anelastic measurement. Assuming that the small anomaly in the χ-versus-T curve at 288 K (see figure 7(b)) is attributable to the ordering of Mn^{3+} and Mn^{4+}, the value of T_A under static conditions is determined to be ~290 K.

4.2. Model B: movement of Li^+ ions on the tetrahedral 8a site

The insertion of excess lithium into $LiMn_2O_4$ induces a change in the distribution of Li ions [8, 11]; that is, the distribution of lithium in $LiMn_2O_4$ can be represented as $(Li)_{8a}[Mn_2]_{16d}O_4$, while that of $Li_2Mn_2O_4$ can be represented as $(Li)_{8a}(Li)_{16c}[Mn_2]_{16d}O_4$, where 16c is the vacant octahedral site. Thus, there is a possibility that Li^+ ions can move between the 8a site and the 16c site in $LiMn_2O_4$, though the origin of the phase transition at T_A is most likely the ordering of Mn^{3+} and Mn^{4+} ions on the octahedral 16d site. As a result of the ordering of Mn ions, the distribution of Li^+ ions would be altered to minimize an electrostatic repulsion. Therefore, an external stress could give rise to a rearrangement of Li^+ ions; hence, the Q^{-1} peak just below T_A may be attributable to a stress-induced relaxation of the distributions of Li^+ ions between the 8a site and the 16c site. The activation energy of such a relaxation process would vary with temperature and/or frequency in the vicinity of T_A. This is because the relaxation process depends not only on the distribution of Mn ions but also on the structure of the area between two adjacent MnO_6 layers. If this assumption is true, there should exist a correlation between the Q^{-1} peak and the content of Li^+ ions in $LiMn_2O_4$. Therefore, it is necessary to investigate elastic/anelastic properties of various kinds of the $Li_xMn_2O_4$ samples with $0 \leqslant x \leqslant 2$.

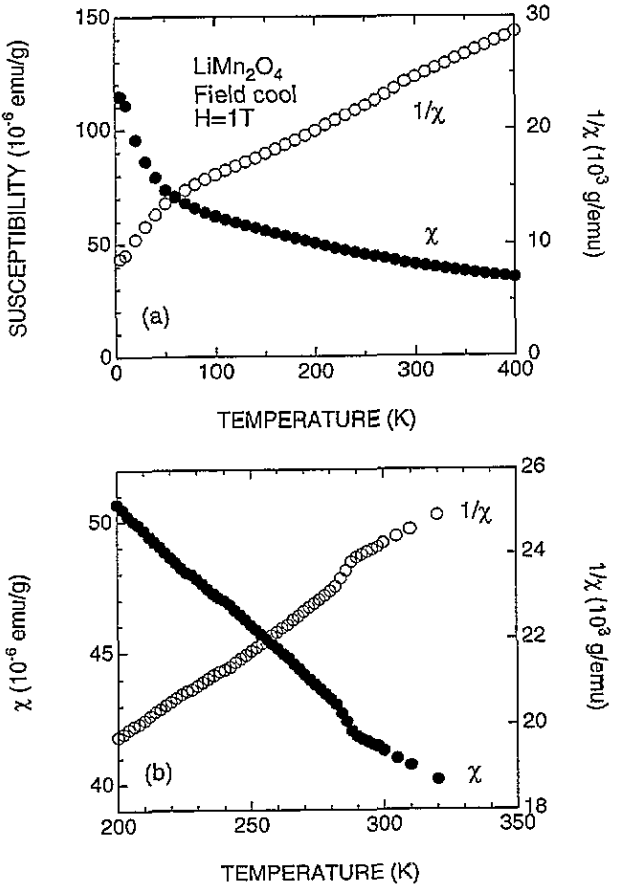

Figure 7. Temperature dependences of (a) the magnetic susceptibility (χ) and $1/\chi$ for $LiMn_2O_4$; χ was measured in a magnetic field of $H = 1$ T; (b) magnification at temperatures in the vicinity of T_A.

5. Summary

Using a vibrating-reed technique, we have measured both the Young's modulus sound velocity (V_E) and the internal friction (Q^{-1}) for a polycrystalline sample of $LiMn_2O_4$ in the temperature range between 35 and 350 K. The temperature dependences of V_E and Q^{-1} are found to be parallel to those for magnetite; the minimum of V_E is observed at around 225 K (T_A) and the peak of Q^{-1} at 210 K (T_{peak}) at the resonance frequency of $f_r(300\ K) = 0.81$ kHz. Furthermore, both the V_E-versus-T curve and the Q^{-1}-versus-T curve shift toward the higher-temperature side by ~45 K and ~20 K, as f_r(300 K) is increased from 1.32 kHz to 2.69 kHz; it should be noted that $T_{peak} < T_A$ for each of the data obtained at different values of f_r. According to the present elastic and magnetic measurements, $LiMn_2O_4$ undergoes a phase transition at around 290 K. This phase transition is probably due to an ordering of Mn^{3+} and Mn^{4+} ions on the octahedral 16d site in the spinel lattice. On the other hand, the origin of the Q^{-1} peak is considered to be caused by a stress-induced relaxation of the distributions of Mn ions or Li ions. However, some discrepancies between this model and the experimental results remain. In order to achieve a further understanding of the mechanism of the phase transition, an NMR study of $LiMn_2O_4$

is in progress.

Acknowledgments

We would like to thank Professor K Fossheim and Dr O M Ness of the Norwegian Institute of Technology for helpful suggestions. We are grateful to Drs N Koshizuka and S Tanaka of SRL-ISTEC for their support, to Mr T Sasaki, Dr T Hioki and Dr S Noda of Toyota CRD Laboratories for their help in the experiment.

Note added in proof. Just after we made our original submission, Yamada and Tanaka [30] reported a structural phase transition at around 280 K for $LiMn_2O_4$ using a differential scanning calorimetric analysis and a powder x-ray diffraction analysis. Their result seems to be consistent with our result.

References

[1] Thackeray M M, David W I F, Bruce P G and Goodenough J B 1983 *Mater. Res. Bull.* **18** 461
[2] Desilvetro J and Haas O 1990 *J. Electrochem. Soc.* **137** 5C and references therein
[3] Scrosati B 1992 *J. Electrochem. Soc.* **139** 2776 and references therein
[4] Ohzuku T 1994 *Lithium Batteries* ed G Pistoia (Amsterdam: Elsevier Science) pp 239-80 and references therein
[5] *Joint Committee on Powder Diffraction Standards* 1986 (International Center for Diffraction Data, Swarthmore) No 35-782
[6] Wickham D G and Croft W J 1958 *J. Phys. Chem. Solids* **7** 351
[7] Hunter J C 1981 *J. Solid State Chem.* **39** 142
[8] Mosbah A, Verbaere A and Tournoux M 1983 *Mater. Res. Bull.* **18** 1375
[9] David W I F, Thackeray M M, Bruce P G and Goodenough J B 1984 *Mater. Res. Bull.* **19** 99
[10] Thackeray M M, Johnson P J, de Picciotto L A, Bruce P G and Goodenough J B 1984 *Mater. Res. Bull.* **19** 179
[11] David W I F, Thackeray M M, de Picciotto L A and Goodenough J B 1987 *J. Solid State Chem.* **67** 316
[12] Fraser D B 1968 *Physical Acoustics V* ed W P Mason (New York: Academic) pp 59–110
[13] Nowick A S and Berry B S 1972 *Anelastic Relaxation in Crystalline Solids* (New York: Academic)
[14] Barmatz M and Golding B 1974 *Phys. Rev.* B **9** 3064
[15] Mukhopadhyay P K and Raychaudhuri A K 1987 *J. Phys. E: Sci. Instrum.* **20** 507
[16] Ness O M, Fossheim K, Motohira N and Kitazawa K 1991 *Physica* C **185–189** 1391
[17] Sugiyama J, Isawa K and Yamauchi H 1995 *Physica* C **242** 163
[18] Kingery W D, Bowen H K and Uhlmann D R 1976 *Introduction to Ceramics* 2nd edn (New York: Wiley) pp 773–7
[19] Gibbons D F 1957 *J. Appl. Phys.* **28** 810
[20] Ledbetter H M, Austin M W, Kim S A and Lei Ming 1987 *J. Mater. Res.* **2** 786
[21] Shindo Y, Ledbetter H M and Nozaki H 1995 *J. Mater. Res.* **10** 7
[22] Verwey E J W and Haayman P W 1941 *Physica* **8** 979
[23] Fine M E and Kenney N T 1954 *Phys. Rev.* **94** 1573
[24] Kamigaki K 1961 *J. Phys. Soc. Japan* **16** 1170
[25] Smit J and Wijn H P J 1959 *Ferrites* (New York: Wiley) and references therein
[26] Goodenough J B, Manthiram A and Wnetrzewski B 1993 *J. Power Sources* **43–44** 269
[27] Schütte L, Colsmann G and Reuter B 1979 *J. Solid State Chem.* **27** 227
[28] Melcher R L 1976 *Physical Acoustics XII* ed W P Mason and R N Thurston (New York: Academic) pp 1–77 and references therein
[29] Kaplan M D and Vekhter B G 1995 *Cooperative Phenomena in Jahn–Teller Crystals* (New York: Plenum) and references therein
[30] Yamada A and Tanaka M 1995 *Mater. Res. Bull.* **30** 715